Structural, morphological and optical properties of Mn doped ZnS nanocrystals

(Propriedades estruturais, morfológicas e ópticas de nanocristais de ZnS dopado com Mn)

V. D. Mote[1], Y. Purushotham[2], B. N. Dole[1*]
[1]Advanced Materials Research Laboratory, Department of Physics, Dr. B. A. Marathwada University, Aurangabad-431 004, India
[2]Centre for Materials for Electronics Technology, IDA Phase-III, Cherlaplly, Hyderabad-500 051, India
dolebn_phys@yahoo.in

Abstract

Mn doped ZnS samples with composition formula $Zn_{1-x}Mn_xS$ where x = 0.00, 0.02, 0.05 and 0.10 were prepared by chemical method. Samples characterized for its structural, morphological and optical properties by X-ray diffraction (XRD), transmission electron microscopy (TEM), Fourier transform infrared spectroscopy (FTIR) and UV–vis spectrometer. XRD patterns confirm cubic zinc blend structure with no secondary phases for pure and Mn doped ZnS. Lattice constant value increases slightly with Mn concentration due to the substitution of Mn in ZnS lattice. TEM images show that the particles have spherical in shape with an average particle size between 3-4 nm. The chemical species of the grown crystals are identified by FTIR spectra. Optical absorption spectra show decrement in band gap with increasing Mn concentration.
Keywords: ZnS, nanocrystals, particle size, surface morphology, optical properties.

Resumo

Amostras de ZnS dopadas com Mn de composição $Zn_{1-x}Mn_xS$, x = 0, 0,02, 0,05 e 0,10 foram preparadas por método químico e caracterizadas estructural, morfológica e ópticamente por difração de raios X (DRX), microscopia eletrônica de transmissão e espectroscopia no infravermelho (FTIR) e espectrofotometria de absorção óptica UV–VIS. Os difratogramas de raios X confirmam a estrutura cúbica sem fases secundárias no ZnS puro e no dopado. O valor do parâmetro de rede com o aumento na concentração de manganês devido à substituição do manganês na rede do ZnS. Imagens de microscopia eletrônica de transmissão mostram que as partículas são esféricas com tamanho médio 3-4 nm. As espécies químicas no cristal foram identificadas pelos espectros FTIR. Os espectros de absorção óptica mostram decréscimo no gap da banda com o aumento da concentração de Mn.
***Palavras-chave**: ZnS, nanocristais, tamanho de partícula, morfologia de superfície, propriedades ópticas.*

INTRODUCTION

Semiconductor nanocrystals have been extensively studied by scientists owing to their potential applications in recent years [1, 2]. Zinc sulfide is an important material owing to numerous applications. The theoretical band gap of this II-VI compound semiconductor is 3.6 eV [3]. Behavior of these materials is different from bulk semiconductors due to increase in particle size, band structure changes, increase in band gap and edges of the band split into discrete energy levels. Divalent substitution such as Mn^{2+}, Cu^{2+} and Ag^{2+} with ZnS semiconductors and their photo physical and photochemical properties were investigated [4-9]. The photoluminescence mechanism of ZnS nanocrystals doped with other metal ions is very complex. Smaller particles have higher surface to volume ratio and more surface state therefore contain more accessible carriers for photoluminescence [10]. This indicates that surface state is very important to the physical properties, especially the optical properties of nanoparticles. Divalent elements like Mn^{2+} ions doped ZnS nanocrystals can be obtained in many ways such as spray-based method [11], mechanochemical route [12], ultrasonic radiation of solution [13], Gama irradiation method [14], chemical precipitation method [15], organic metallic method [16], polymerization [17], reverse Michelle method [18] and sol-gel method [19]. We preferred chemical method for the preparation of Mn doped ZnS nanocrystals to get the cluster formation. This method is simple, low cost and availability of the equipments.

The aim of this work is to study the effect of Mn^{2+} ions doping on synthesis, structural, morphological and optical properties of ZnS nanoparticles. Characterization techniques employed to characterize the materials were UV-Visible, XRD and TEM. Crystal structure and average grain size were measured using XRD. TEM used to study particle size and morphology. FTIR used to study quantum size effect in ZnS nanoparticles.

EXPERIMENTAL

Samples with chemical formula $Zn_{1-x}Mn_xS$, where x = 0.00, 0.02, 0.05 and 0.10, were prepared by chemical method using manganese acetate, Zinc acetate and sodium sulfide in aqueous medium without using any other reagent. In this, 20 mL of 1M zinc acetate solution was diluted to 80 mL using distilled water and 20 mL of manganese acetate solution was added dropwise, followed by drop wise addition of 20 mL of 1M sodium sulfide under vigorous stirring to obtain pH 13.5. A white precipitate was obtained which was separated by centrifugation. The precipitate was washed several times with water and ethanol. The precipitate was then dried under vacuum at 60 °C to get the powder samples. Mn doped-ZnS nanocrystals were prepared at room temperature by mixing calculated amounts of zinc acetate solution and manganese acetate solution followed by dropwise addition of saturated solution of Sodium sulfide up to pH 13.5. The mixture was vigorously stirred for 2 h. The precipitate was filtered from the reaction mixture and washed several times with ethanol to remove all sodium particles. The wet precipitate was then dried. The samples were characterized by X-ray diffraction (PW-3710), Transmission electron microscopy (TEM), FTIR spectroscopy (JASCO FTIR-4100) and UV-VIS spectroscopy.

RESULTS AND DISCUSSION

X-ray diffraction study

X-ray diffraction (XRD) patterns of the synthesized ZnS and Mn doped ZnS samples are shown in Fig. 1. All XRD peaks are matched well with JCPDS No. 77- 2100 and were indexed as cubic Zinc blend structure. It can be seen from the figure that XRD peaks are broadened with three main peaks corresponding to (111), (220) and (311) planes. Mn doped ZnS samples also showing Zinc blend structure of ZnS which confirms the formation of Mn doped ZnS solid solution and there is no formation of Mn precipitation or secondary phases. Youn et al. [24] reported that for higher concentration of Mn doping in ZnS results separation of Mn atoms from the ZnS matrix.

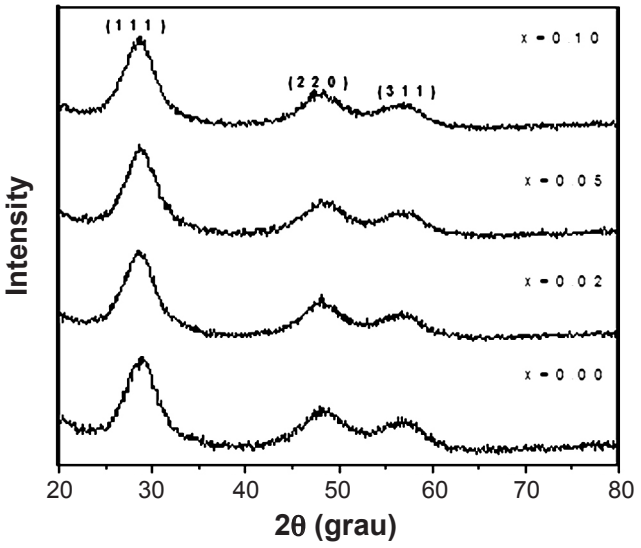

Figure 1: X-ray diffraction patterns of Mn doped and undoped ZnS samples.
[Figura 1: Difratogramas de raios X de ZnS e de ZnS dopado com Mn.]

The lattice constant 'a' was calculated using the following relation

$$\frac{1}{d_{hkl}^2} = \left(\frac{h^2 + k^2 + l^2}{a^2}\right) \quad \text{(A)}$$

We observed that 'a' slightly increases for Mn doped nanocrystals as shown in Fig. 2. This may be due to the substitution of Mn^{2+} ions in Zn^{2+} ions. Since the ionic radius of Mn^{2+} ion (0.80 A^0) is larger than that of Zn^{2+} ion (0.74 A^0). The volume of unit cell was calculated using the lattice parameter 'a' and it is found that the unit of volume cell enhances with increasing Mn concentration as shown in Fig. 3. This indicates that Mn^{2+} ions go to Zn site in the structure due to larger ionic radius. The values of volume of unit cell are tabulated in Table I. X-ray density was calculated using the following relation.

Table I - Lattice constant, crystallite size, volume of unit cell and X-ray density of Mn doped ZnS nanocrystals.
[Tabela I - Constante de rede, tamanho de cristalito, volume da célula unitária e densidade (DRX) de nonocristai de ZnS dopados com Mn.]

Samples	a (Å)	crystallite Size (nm)	Volume (Å)^3	X- ray density (g/cm^3)
0.00	5.3706	02.89	154.91	4.1772
0.02	5.3711	02.65	154.95	4.1671
0.05	5.3725	02.57	155.07	4.1505
0.10	5.3734	02. 50	155.15	4.1261

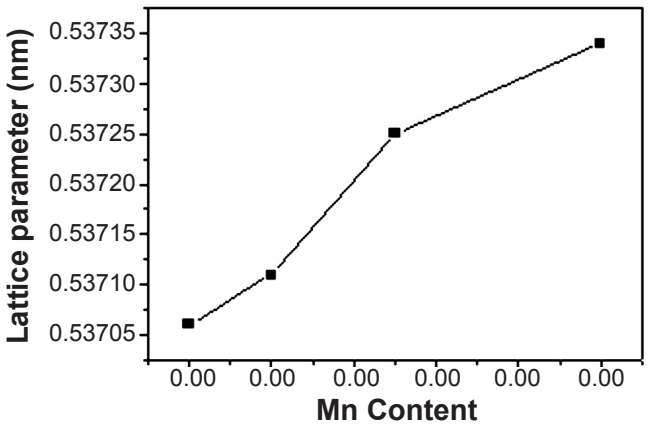

Figure 2: Lattice parameter Vs Mn content of pure and Mn doped ZnS samples.
[Figura 2: Parâmetro de rede de ZnS e de ZnS dopado com Mn.]

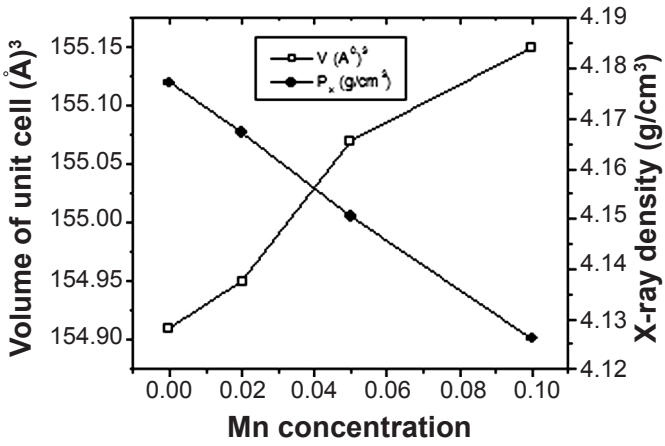

Figure 3: Volume of unit cell and X-ray density with Mn content of ZnS samples.
[Figure 3: Volume da célula unitária e densidade (DRX) em função do teor de Mn.]

$$\rho_x = \frac{nM}{N_A V} \qquad (B)$$

where n is number of atoms per unit cell, M is molecular weight of the samples, N_A is Avogadro's number and V is unit cell volume. The values of X-ray density are also tabulated in Table I. X-ray density decreases with increasing Mn concentration. This decrease was attributed to the decrease in molecular weight. Since atomic weight of Mn ion (58.93 amu) is smaller than that of Zn ion (65.37 amu). The plots of unit cell volume and X-ray density with Mn content are shown in Fig. 3.

The average crystallite size of Mn doped ZnS samples was determined by extra broadening of the X-ray diffraction peaks of the samples using the Debye-Scherrer's formula using following relation

$$D = \frac{K\lambda}{\beta_{hkl} \text{Cos}\ \theta} \qquad (C)$$

where D is the crystallite size, K is the shape factor (0.9), λ is the wavelength of Cuk_α radiation, β_{hkl} is the instrumental corrected integral breadth of the reflection (in radians) located at 2θ and θ is the angle of reflection (in degree). It is found that the average crystallite size is in the range of 3-2 nm and values are depicted in Table I. It is observed that the average crystallite size decreases with increasing Mn concentration. It means the Zn^{2+} ions are replaced by Mn^{2+} ions in the ZnS matrix. It may be due to the induced growth of the particles and enhancement of surface area to volume ratio in the system.

Morphological studies

It is necessary to know an exact particle size and structures of nanomaterials by direct measurement, such as transmission electron microscope (TEM), which can reveal the particle size, shape and orientation of the Mn doped ZnS nanoparticles. Electron diffraction patterns at different regions on the TEM grid were recorded for pure ZnS sample. We did not find any other diffraction rings that cannot be indexed by sphalerite structure. Fig. 4a shows TEM image of pure ZnS sample. TEM image shows that particles are nearly in spherical shape and having average particle size of 3-4 nm for the pure ZnS sample. This value is consistent with the XRD result of pure ZnS sample. Fig. 4(b) shows the corresponding selected area electron diffraction (SAED) pattern. The SAED pattern corresponds to reflections from three crystal planes which indicate (111), (220) and (311). It is observed that the particles are well separated and evidenced with few agglomerations.

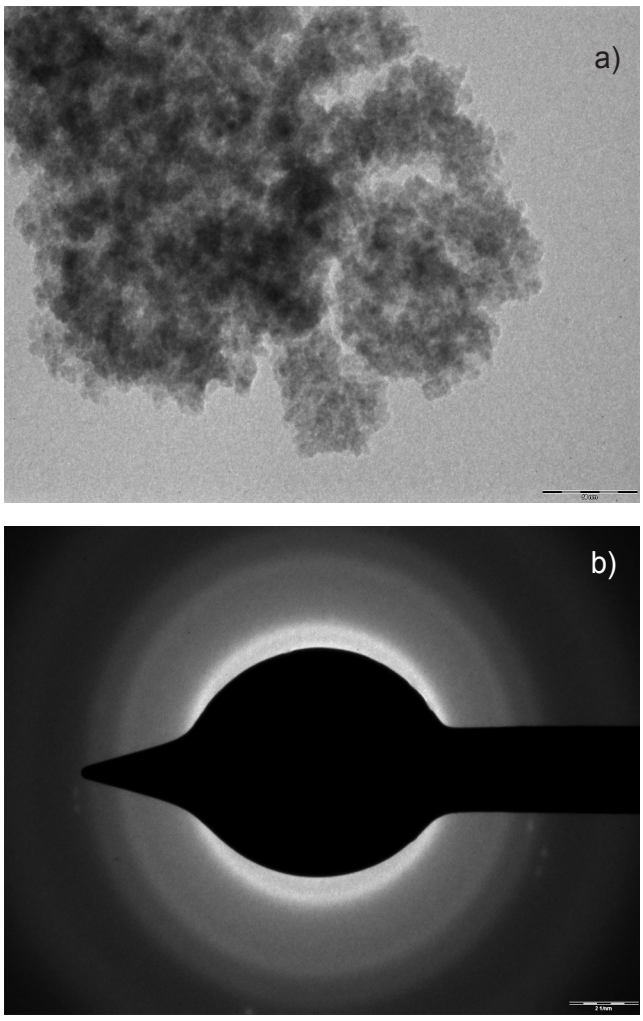

Figure 4: Transmission electron microscope image (a) and Selected Area Electron Diffraction (SAED) image of ZnS nanocrystals.
[Figura 4: Imagens de microscopia eletrônica de transmissão (a) e difrão de elétrons de área selecionada (b) de nanocristais de ZnS.]

The agglomeration was probably due to the particles in a concentrated sample could end up in association during grid drying in the TEM sample processing protocol [25]. The spherical shape of the particles is also evidenced from the Fig. 4b, which presents magnified view of nanocrystals.

Table II - Assignment of frequencies of FTIR spectra of Mn doped ZnS nanocrystals.
[Tabela II - Frequências dos espectros FTIR de nanocristais de ZnS dopados com Mn.]

x=0.00 (cm^{-1})	x=0.02 (cm^{-1})	x=0.05 (cm^{-1})	x=0.10 (cm^{-1})	Assignment of frequencies
439.60	404.59	439.60	483.87	Asymmetric bending
668.15	658.88	668.15	658.88	ZnS stretching
913.18	903.91	905.68	921.421	Additional asymmetric stretching
1008.92	1027.45	1027.45	1018.18	Shoulder with asymmetric stretching
1219.97	1228.20	1219.97	1245.71	Symmetric stretching
1350.72	1350.72	1350.72	1350.72	Weak additional stretching
1420.73	1429.99	1429.99	1420.73	C=O Asymmetric stretching
1561.77	1552.50	1561.77	1570.00	C=O Symmetric stretching
2350.37	2358.61	2358.61	2358.51	Weak additional bands
3436.51	3427.25	3506.52	3436.51	O-H stretching

FTIR study

Fig. 5 shows FTIR spectra of pure and Mn doped ZnS samples. The values of IR peaks of all samples are tabulated in Table II. It clearly shows a broad peak at 3400-3600 cm^{-1} due to O-H stretching has been observed in all samples because of some absorbed moisture.

The samples at room temperature show characteristic peaks at 612, 865, 1004, 1119, and some other associated peaks are shown in Fig. 5. It is observed that the peak at 612 cm^{-1} is assigned to the ZnS band (i.e. corresponding to sulfides) for all samples. FTIR spectra of our samples yield the bands which are in good agreement with the reported values [26]. The change is observed in values when Mn content is increased it means that the formation of nanophase in the prepared samples. IR absorption peaks at 900-1500 cm^{-1} are due to the oxygen stretching and bending frequency. The additional weak bands and shoulders at 2941, 2847, 2353, 1634 and 1409 cm^{-1} are observed. It may be due to the microstructure formation of the samples. Bands around 1200 and 1100 cm^{-1} are due to the characteristics frequency of inorganic ions. Due to low temperature, weak additional bands are observed at 992, 984 and 865 cm^{-1}. These modes indicate the presence of resonance interaction between vibrational modes of sulfide ions in the crystals [27].

Optical studies

The absorption spectra of pure and Mn doped ZnS samples are shown in Fig. 6. The absorption spectra of Mn doped samples are different than of undoped sample. It is due to effect of doped ions on band structure of the host material. The absorption peaks and edges of the samples vary with changing in the molar concentration of Mn^{2+} ions. ZnS has good absorption for light in the wave length of 220-350 nm [28]. Semiconductor crystallites in the diameter range of a few nanometers show a three dimensional quantum size effect in their electronic structure. The quantum size effects on the band gap absorption energy can be measured by UV-Vis absorption spectroscopy.

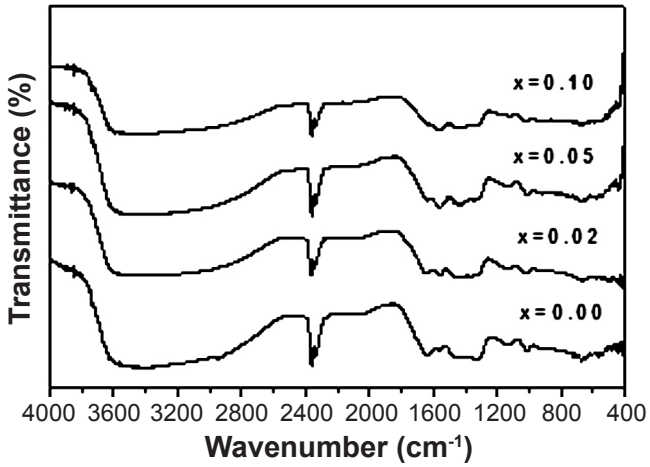

Figure 5: FTIR spectra of pure and Mn doped ZnS nanocrystals.
[Figura 5: Espectros FTIR de nanocristais de ZnS puro e dopado com Mn.]

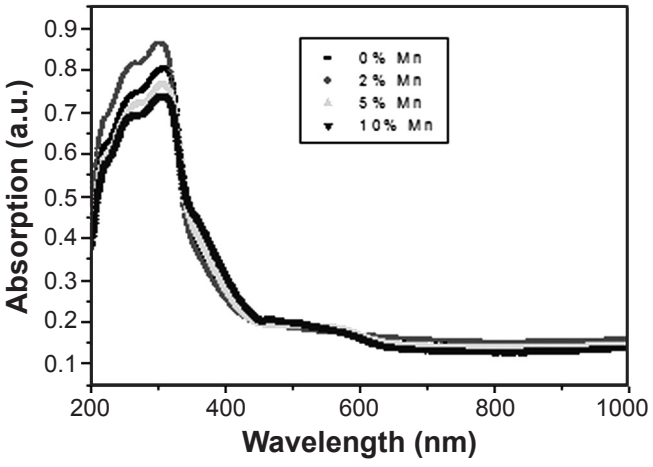

Figure 6: UV-VIS spectra of pure and Mn doped ZnS samples.
[Figura 6: Espectros UV-VIS de amostras de ZnS pura e dopada com Mn.]

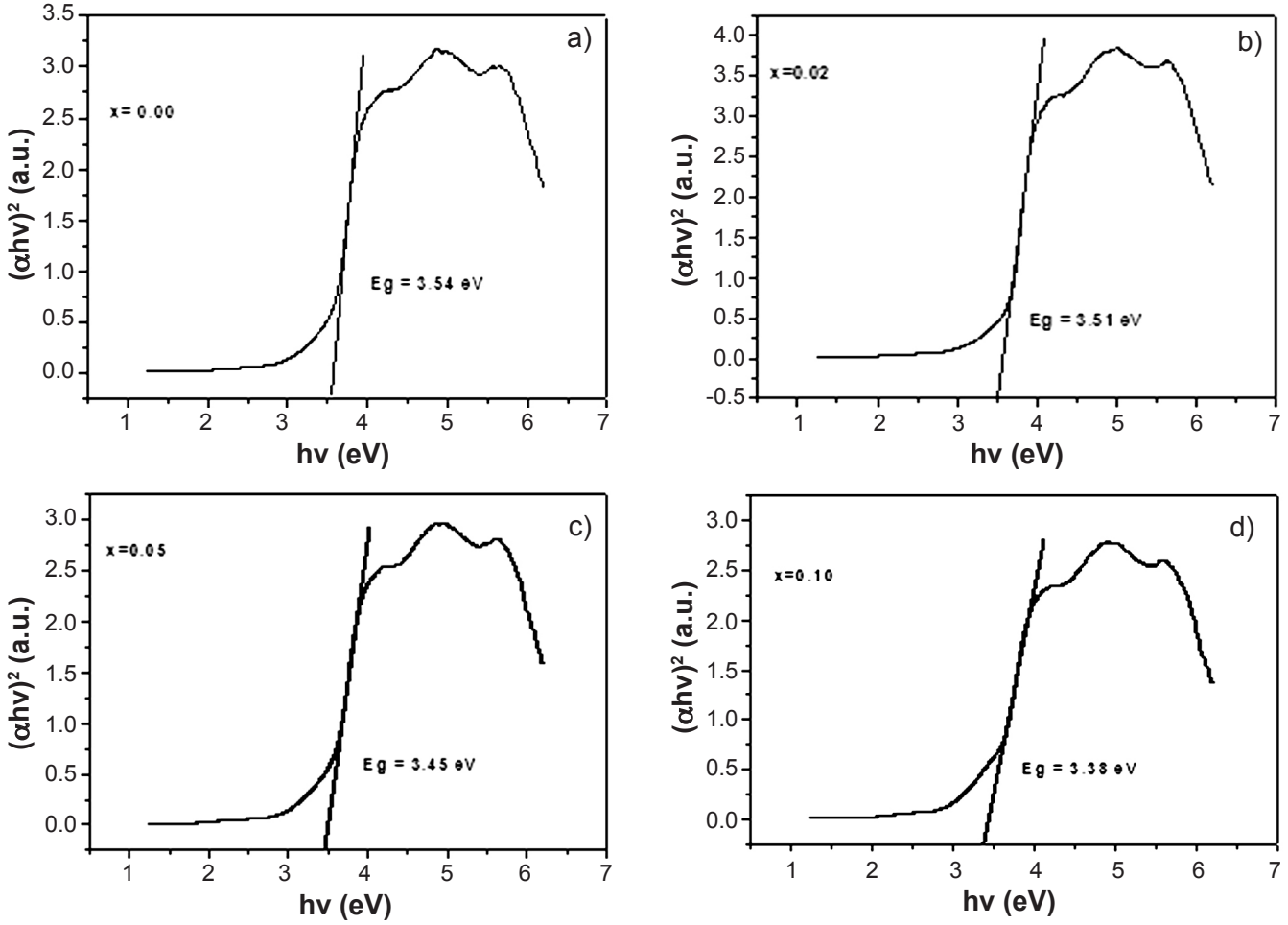

Figure 7: The plots of $(ah\nu)^2$ vs. photon energy of Mn doped and undoped ZnS samples.
[Figura 7: Gráficos de $(ah\nu)^2$ vs. energia do fóton de amostras de ZnS pura e dopada com Mn.]

It is well known that the cubic ZnS is a direct gap semiconductor [29]. The relation between the absorption coefficient (α) and incident photon energy (hν) allowed direct transition is [30]:

$$\alpha h\nu = A(h\nu - E_g)^{1/2} \qquad (D)$$

where A is the constant and E_g is the energy band gap of the material.

The plots of $(\alpha h\upsilon)^2$ versus hυ for the undoped ZnS and Mn doped ZnS nanocrystals are represented in Fig. 7. By extra plotting the straight portion of the graph on hυ axis at α = 0, it is found that the band gap of the undoped and Mn doped ZnS nanoparticles for concentrations 0.00, 0.02, 0.05 and 0.10 to be 3.54, 3.51, 3.45 and 3.38 eV, respectively. These values can be compared with band gap values of 3.38-3.54 eV at room temperature for bulk ZnS [31]. From figure, it is noted that the absorption edges slightly shifted towards the lower energy side with increasing Mn upto 10%. The band gap is found to decrease with increasing Mn concentration as shown in Fig. 8. The same shifts of the absorption edge with increasing Mn concentration from 0 to 9 at % at fixed size of ZnS nanoclusters were reported in literature [32, 33].

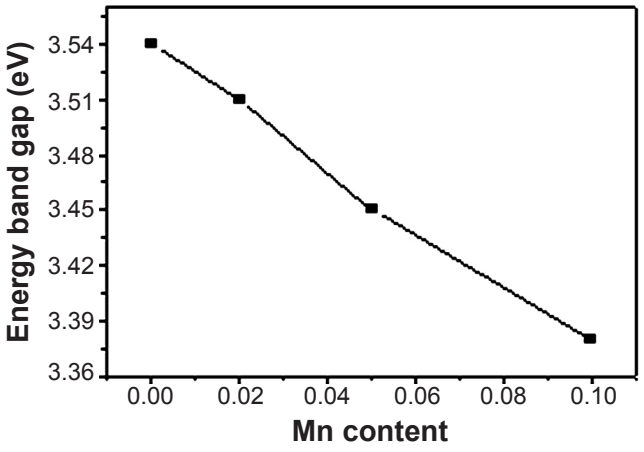

Figure 8: Energy band gap vs. Mn content of Mn doped and undoped ZnS samples.
[Figura 8: Gap da banda de energia vs. teor de Mn em amostras de ZnS pura e dopadas.]

But the variation of the band gap with the Mn concentration is the opposite is observed in Mn doped CdS nanocluster [34]. Levy et. al. reported that a minimum energy band gap was observed for 5-8% of Mn concentration CdS samples. These changes of the band gap with Mn concentration are

due to exchange interaction in confined region.

In our case, the size of ZnS nanoparticles were found to be in the range of 2-4 nm which is same as the exciton Bohr radius (2.1nm) for a cubic ZnS structure. Hence the slight change of band gap may be assigned to weak quantum confinement effect in ZnS clusters. This small change in the band gap suggests that there is direct energy transfer between the semiconductor-excited states and the 3d levels of Mn^{2+} ions [35].

CONCLUSIONS

The Mn doped ZnS nanocrystals were synthesized by a chemical method at room temperature. XRD patterns suggest that Mn ions go to Zn sites in the crystals without changing the Cubic structure. The lattice parameter slightly increases with increasing Mn concentration. We also observed that the average crystallite size is reduced with increasing Mn concentration; it may be due to a small grain growth in comparison with undoped ZnS nanocrystals. No secondary phases were observed upto 10% of Mn doped ZnS samples. It indicate that the homogenous substitution of Mn ions into the ZnS lattice structure. The TEM image of pure ZnS nanocrystals exhibits an average particle size of about 3-4 nm. The TEM result is in good agreement with results of XRD. FTIR analysis confirms the formation of ZnS and Mn doped ZnS samples. The UV-VIS measurement shows the reduction in the band gap with increasing Mn content. It may be due to the direct energy transfer between the semiconductor-excited states and the 3d levels of Mn^{2+} ions.

ACKNOWLEDGEMENT

B. N. Dole would like to thank University Grants Commission, New Delhi, India for financial assistance (Project No. F-37-563/2009/SR) and Prof. S. S. Shah for his encouragement.

REFERENCES

[1] H. Weller, Angew. Chem. Int. Ed. Engl. **32** (1993) 41-53.
[2] A. P. Alivisatos, J. Phys. Chem. **100** (1996) 13226-39.
[3] P. Yang, M. Lu, D. Xu, D. Yuan, M. Pan, G. Zhou, Mater. Res. Bull. **36** (2001) 1301-06.
[4]J. Yu, H. Liu, Y. Wang, F. E. Fernandez, W. Jia, J. Lumin. **76-77** (1998) 252-55.
[5] R. N. Bhargava, D. Gallagher, T. Welker, J. Lumin. **60-61** (1994) 275-80.
[6] K. Sooklal, B. S. Cullum, S. M. Angel, C. J. Murphy, J. Phys. Chem. **100** (1996) 4551-55.
[7] G. N. Lvanova, V. A. Kasiyan, N. D. Nedeoglo, D. D. Nedeogle, J. Lumin. **82** (1999) 277-83.
[8] A. A. Khosravi, M. Kundu, L. Jatwa, S. K. Deshpande, U. A. Bhagwat, M. Sastry, S. K. Kulkarni, Appl. Phys. Lett. **67** (1995) 2702-05.
[9] D. Denzler, M. Olschjewski, K. Sattler, Appl. Phys. Lett. **84** (1998) 2841-44.
[10] W. Chen, Z. Wang, Z. Lin, L. Lin, Appl. Phys. Lett. **70** (1997) 1466.
[11] L. Amirav, A. Amirav, E. Lifshitz, J. Phys. Chem. Lett. B **109** (2005) 9857-60.
[12] P. Balaz, E. Boldizarova, E. Godocikova, Briancin, J. Mater. Lett. **57** (2003) 1585-89.
[13] J. F. Xu, H. S. Jiw, Y. W. Tang, Du, Appl. Phys. A **66** (1998) 639-41.
[14] A. H. Souici, N. Keghouche, J. A. Delaire, H. Remita, M. Mostafavi, Chem. Phys. Lett. **422** (2006) 25-29.
[15] H. Yang, P. Hollway, J. Appl. Phys. **93** (2003) 586-93.
[16] J. H. Chung, C. S. Ah, D. J. Jang, J. Phys. Chem. B **105** (2001) 4128-32.
[17] I. Yu, I. Tetsukio, M. Seena, J. Phys. Chem. Solids **57** (1996) 373-79.
[18] K. Manzoor, S. R. Vadera, N. Kumar, T. R. N. Kutty, Mater. Chem. Phys. **82** (2003) 718-25.
[19] N. Karan, R. Suchitra, F. Singh, J. Cryst. Growth **268** (2004) 585-89.
[20] S. J. Xu, S. J. Chua, B. Liu, L. M. Gan, C. H. Chew, G. Q. Xu, Appl. Phys. Lett. **73** (1998) 478-81.
[21] M. Konishi, T. Isobe, M. Senna, J. Lumin. **93** (2001) 1-8.
[22] L. X. Cao, J. H. Zhang, S. L. Ren, S. H. Huang, Appl. Phys. Lett. **80** (2002) 4300-03.
[23] M. W. Wang, L. D. Sun, C. H. Liu, C. S. Liao, C. H. Yan, Chin, J. Lumin. **20** (1999) 247.
[24] H. J. Yuan, X. Q. Yan, Z. X. Zhang, D. F. Liu, Z. P. Zhou, L. Cao, J. X. Wang, Y. Gao, L. Song, L. F. Liu, X. W. Zhao, X. Y. Dou, W. Y. Zhou, S. S. Xie, J. Cryst. Growth **271** (2004) 403-08.
[25] I. Chakraborty, S. P. Moulik, J. Nanopart. Res. **7** (2005) 237.
[26] B. S. Rema Devi, R. Raveendran, A. V. Vaidyan, Parama-J. Physics **68** (2007) 679-87.
[27] S. K. kurian, S. Sebastian, J. Mathew, K. C. George, Ind. J. Pure Appl. Phys. **42** (2004) 926-33.
[28] C. Jianfeny, L. Yaling, W. Yuhong, Y. Jimmy, C. Dapeng, Mater. Res. Bull. **39** (2004) 185-94.
[29] S. Sapra, N. Shanthi, D.D. Sarma, Phys. Rev. B 66 (2002) 205202-10.
[30] J. I. Pankove, "Optical Process in Semiconductors", Prentice-Hall Inc., USA, 36 (1971).
[31] B. Y. Geng, X. W. Liu, Q. B. Du, X. W. Wei, L. D. Zhang, Appl. Phys. Lett. **88** (2006) 163104-07.
[32] S. Sarpa, J. Nanda, A. Nanda, A. Anand, S.V. Bhat, D. D. Sarma, J. Nanosci. Nanotech. **3** (2003) 392.
[33] B. Bhattacharlee, D. Ganguli, K. Lakoubovskii, A. Stresmans, S. Chaudhari, Bull. Mater. Sci. **25** (2002) 175-80.
[34] L. Levy, J. F. Hochepied, M. P. Pileni, J. Phys. Chem. **100** (1996) 18322-26.
[35] F. J. Brieler, M. Froba, L. Chem, P. J. Klar, W. Heimbrodt, H. A. Krug, V. Nidda, A. Loidl, Chem. Eur. J. **81** (2002) 185.
(Rec. 06/11/2012, Ac. 25/06/2013)